Available online at https://link.springer.com/journal/42241
http://www.jhydrodynamics.com
Journal of Hydrodynamics, 2024
https://doi.org/10.1007/s42241-024-0018-6

Numerical simulation of liquid sloshing in a spherical tank by MPS method

Cong-yi Huang[1], Ji-fei Wang[2], Wei-wen Zhao[1], De-cheng Wan[1*]
1. *Computational Marine Hydrodynamic Lab (CMHL), School of Naval Architecture, Ocean and Civil Engineering, Shanghai Jiao Tong University, Shanghai 200240, China*
2. *Shanghai Aerospace System Engineering Institute, Shanghai 201109, China*

(Received February 20, 2024, Revised April 18, 2024, Acceped April 22, 2024, Published online May 10, 2024)

Abstract: This paper investigates the sloshing phenomena in a spherical liquid tank using the moving particle semi-implicit (MPS) method, a crucial study in fluid dynamics. Distinct from previous research focused on rectangular or LNG tanks, this work explores the unique motion patterns inherent to spherical geometries. The accuracy of our in-house MPS solver MLParticle-SJTU is validated against experimental data and finite volume method (FVM). And the MPS method reveals a closer alignment with experimental outcomes, which suggests that MPS method is particularly effective for modeling complex, non-linear fluid behaviors. Then the fluid's response to excitation at its natural frequency is simulated, showcasing vigorous sloshing and rotational motion. Detailed analyses of the fluid motion are conducted by drawing streamline diagrams, velocity vector diagrams , and vorticity maps. The fluid's motion response is explored using both time-domain and frequency-domain curves of the fluid centroid, as well as the sloshing force.

Key words: Moving particle semi-implicit (MPS) method, spherical tank, liquid sloshing, model experiment

0. Introduction

Sloshing in liquid tanks refers to the fluctuation phenomena of liquid within partially filled tanks under external excitation. The presence of a free surface introduces significant randomness and non-linearity to these fluctuations, often accompanied by complex phenomena such as wave overturning and surface breaking. This phenomenon is prevalent in practical engineering applications, notably in the liquid tanks of spacecraft fuel storage, where the motion of the spacecraft induces sloshing. Similar occurrences are observed in the liquid tanks of liquid cargo ships. Such sloshing not only exerts considerable impact pressure on the tank walls, potentially affecting structural safety, but it can also induce dynamic instability, impacting the operation of control systems. Therefore, accurate simulation of liquid sloshing and the prediction of sloshing forces are of paramount importance.

Considerable research has been conducted on the sloshing problems in liquid tanks. Lu et al.[1] primarily explored the dynamic model of large-amplitude liquid sloshing in a gravity environment, which extended the moving pulsating ball model for large liquid sloshing to account for gravity effects. Ding et al.[2] employed the finite element method to establish a versatile numerical program for computing the natural frequencies, modes, and dynamic characteristics of liquid sloshing within arbitrary 3-D containers. This research analyzed the results of liquid sloshing under forced excitation and proposes a methodology for creating an equivalent mechanical model for liquid sloshing under external forces. Liu et al.[3] simulated the sloshing of liquid hydrogen in a cryogenic storage tank using the volume of fluid method. A numerical model was established, incorporating environmental heat leakage and phase change at the free interface. The results obtained from this model demonstrated an error of less than 5% when compared with experimental data. Furuichi et al.[4] provided a numerical analysis of liquid surfaces in storage tanks under low-gravity conditions. It emphasized the dynamic behavior of the liquid surface and displacement of the contact line on the solid wall, with experimental data from cylindrical containers in a drop tower. Hari et al.[5] focused on the coupled slosh-vehicle dynamics of a rigid body in atmospheric flight carrying a sloshing liquid, considering the sloshing motion as a simple pendulum and provides stability analysis of this multibody system

Project supported by the National Natural Science Foundation of China (Grant No. 52131102), the National Key Research and Development Program of China (Grant No. 2022YFC2806705).
Biography: Cong-yi Huang (1998-), Female, Ph. D.,
E-mail: cyhuang@sjtu.edu.cn
Corresponding author: De-cheng Wan,
E-mail: dcwan@sjtu.edu.cn

model. Yang et al.[6] discussed a high-fidelity algorithm for the kinematics and dynamics of interfaces in liquid propellant tanks. It highlighted the importance of accurate modeling of interfacial flows, especially when surface tension forces are significant. Chiba et al.[7] studied the dynamic stability of a liquid in a hemispherical tank covered with a plane diaphragm under vertical excitation both theoretically and experimentally.

The studies mentioned above have relied on grid-based methods predominantly. However, for sloshing phenomena characterized by strong non-linearity and significant free surface deformation, grid-based methods may struggle to accurately capture surface deformation and breakage, often leading to mesh distortion. In this context, mesh-free particle methods based on the Lagrangian approach exhibit unique advantages. Numerous researchers have utilized mesh-free methods to simulate liquid tank sloshing. Li et al.[8] investigated the sloshing effects from baffle and non-baffled water tank under different external excitation frequencies and amplitudes using the Weakly Compressible Moving Particle Explicit method. Martinez-Carrascal et al.[9] employed the smoothed particle hydrodynamics (SPH) to develop a simplified model for predicting liquid-induced dissipation under varying liquid viscosities, surface tensions, and tank fill levels. Green et al.[10] used the SPH method with the open-source code DualSPHysics to simulate sloshing phenomena in rectangular, cylindrical, spherical, and annular tanks, achieving results that closely align with analytical solutions. Kotsarinis et al.[11] simulated the liquid sloshing relevant for aerospace engineering purposes using DualSPHysics solver.

The aforementioned studies have primarily used the SPH method. The MPS method, initially proposed by Koshizuka et al.[12], differs from SPH in that it implicitly solves the pressure Poisson equation to obtain pressure, whereas SPH derives particle pressure through state equations. Consequently, the MPS method exhibits greater stability in solving flow field pressures and allows for larger time steps compared with SPH. Our research group has independently developed the MPS-based solver MLParticle-SJTU, which has been applied to simulate various intense free-surface flows, such as dam break problems[13-15], water entry problems[16-17], and fluid structure interaction problems[18-23]. We have also conducted extensive research on liquid sloshing. Wen et al.[24-25] simulated multi-layer-liquid sloshing by the multi-phase MPS method. Xie et al.[26] simulated liquid sloshing inside a liquid tank with elastic baffles. Zhang et al.[27] and Huang et al.[28] simulated the sloshing in the vertically excited liquid tank and captured the Faraday wave.

In this paper, we simulate the sloshing phenomena inside a spherical tank under horizontal excitation using the MPS method. Initially, experimental methods and the FVM approach are utilized to simulate the same conditions for comparison and validation of the MPS method's accuracy. The simulation results reveal that when the excitation frequency matches the tank's natural frequency, the liquid inside the spherical tank exhibits rotational motion. Streamline diagrams, velocity vector maps, and vorticity maps are drawn to analyze the flow field in detail. The time history of the fluid centroid's position and the sloshing force are recorded and analyzed.

1. Numerical methods

Our group has extensively refined the MPS method to enhance its computational efficiency and accuracy. These advancements have enabled the exploration of numerous intricate flow phenomena. The methodology adopted in this work has been comprehensively documented in prior publications[13-15]. Consequently, only a succinct overview of the MPS method will be presented here.

1.1 *Governing equations*

The foundational equations of the MPS method are outlined as Eqs. (1), (2), encompassing the essential fluid dynamics parameters.

$$\frac{1}{\rho}\frac{\mathrm{D}\rho}{\mathrm{D}t} = -\nabla \cdot \boldsymbol{V} = 0 \tag{1}$$

$$\frac{\mathrm{D}\boldsymbol{V}}{\mathrm{D}t} = -\frac{1}{\rho}\nabla p + \nu\nabla^2\boldsymbol{V} + \boldsymbol{g} \tag{2}$$

where ρ is the fluid density, $\boldsymbol{V}$ is the velocity vector, p is the pressure, ν is the kinematic viscosity, $\boldsymbol{g}$ is the gravitational acceleration vector and t is the time.

1.2 *Particle interaction models*

Within the MPS framework, particles interact via a kernel function. The specific kernel function utilized in this study is represented by Eq. (3):

$$W(r) = \frac{r_e}{0.85r + 0.15r_e} - 1, \quad 0 \le r < r_e \tag{3a}$$

$$W(r) = 0, \quad r_e \le r \tag{3b}$$

where $W(r)$ is the kernel function, r is the inter-particle distance, r_e is the radius of influence.

The discretization of terms in the governing equations is achieved through the particle interaction model.

$$\langle \nabla p \rangle_i = \frac{D}{n^0} \sum_{j \neq i} \frac{p_j + p_i}{\left| \boldsymbol{r}_j - \boldsymbol{r}_i \right|^2} (\boldsymbol{r}_j - \boldsymbol{r}_i) W\left(\left| \boldsymbol{r}_j - \boldsymbol{r}_i \right| \right) \tag{4}$$

$$\langle \nabla \cdot \boldsymbol{V} \rangle_i = \frac{D}{n^0} \sum_{j \neq i} \frac{(\boldsymbol{V}_j - \boldsymbol{V}_i) \cdot (\boldsymbol{r}_j - \boldsymbol{r}_i)}{\left| \boldsymbol{r}_j - \boldsymbol{r}_i \right|^2} W\left(\left| \boldsymbol{r}_j - \boldsymbol{r}_i \right| \right) \tag{5}$$

$$\langle \nabla^2 \phi \rangle_i = \frac{2D}{n^0 \lambda} \sum_{j \neq i} (\phi_j - \phi_i) W\left(\left| \boldsymbol{r}_j - \boldsymbol{r}_i \right| \right) \tag{6}$$

$$\lambda = \frac{\sum_{j \neq i} W\left(\left| \boldsymbol{r}_j - \boldsymbol{r}_i \right| \right) \left| \boldsymbol{r}_j - \boldsymbol{r}_i \right|^2}{\sum_{j \neq i} W\left(\left| \boldsymbol{r}_j - \boldsymbol{r}_i \right| \right)} \tag{7}$$

$$\langle n \rangle_i = \sum_{j \neq i} W\left(\left| \boldsymbol{r}_j - \boldsymbol{r}_i \right| \right) \tag{8}$$

where D corresponds to the spatial dimensions, $\boldsymbol{r}$ is the position vector, subscripts i and j are the central particle and the neighbor particle, $\langle n \rangle_i$ is the particle number density and n^0 is the initial particle number density, with the definition as Eq. (8).

1.3 *Pressure Poisson equation*

The pressure within the system is ascertained by resolving the mixed-source term pressure Poisson equation (PPE), drawing upon the approach posited by Tanaka and Masunaga[29], Lee et al.[30].

$$\langle \nabla^2 p^{k+1} \rangle_i = (1-\gamma) \frac{\rho}{\Delta t} \nabla \cdot \boldsymbol{V}_i^* - \gamma \frac{\rho}{\Delta t^2} \frac{\langle n^k \rangle_i - n^0}{n^0} \tag{9}$$

where p^{k+1} signifies the pressure at the $(k+1)$th step, Δt is the time step, $\boldsymbol{V}_i^*$ is the temporal velocity component, γ stands for the weight assigned to the particle number density term, varying from 0 to 1.

1.4 *Free surface detection*

The identification of free surface particles is based on the particle number density. Particles are classified according to the criteria provided in Eqs. (10a)-(10c).

$$\text{If } \frac{\langle n \rangle_i}{n^0} < 0.8 \quad \text{free surface particles} \tag{10a}$$

$$\text{If } \frac{\langle n \rangle_i}{n^0} > 0.97 \quad \text{fluid particles} \tag{10b}$$

$$\text{If } 0.8 < \frac{\langle n \rangle_i}{n^0} < 0.97 \,, \ \langle |\boldsymbol{F}| \rangle_i > 0.9 |\boldsymbol{F}|^0 \quad \text{free surface particles,} \ \langle \boldsymbol{F} \rangle_i = \frac{D}{n^0} \sum_{j \neq i} \frac{\boldsymbol{r}_i - \boldsymbol{r}_j}{\left| \boldsymbol{r}_i - \boldsymbol{r}_j \right|} W\left(\left| \boldsymbol{r}_i - \boldsymbol{r}_j \right| \right) \tag{10c}$$

The value of $\langle |\boldsymbol{F}| \rangle_i$ reflects the asymmetry in the distribution of neighbouring particles. $|\boldsymbol{F}|^0$ is designated as the initial value of for surface particles.

1.5 *Calculation model preprocessing*

In this study, we optimize the preprocessing of particle distribution for simulating the sloshing in a spherical liquid tank. Traditionally, the preprocessing module of DualSPHysics distributes particles uniformly within the computational domain by placing them on grid points, later classifying them as fluid or boundary particles based on their proximity to the boundaries. However, this method results in an unsmooth, jagged boundary representation for spherical tanks, as the particles may not align precisely with the tank's circumference, as shown in Fig. 1(a). To address this, we introduced a novel approach using the Fibonacci sequence for generating a uniformly distributed particle model on the surface of the spherical tank. The Fibonacci sequence, characterized by each number being the sum of the two preceding ones, inherently aligns with the golden ratio, commonly found in natural patterns. This natural alignment offers an ideal solution for uniform particle distribution. By integrating the Fibonacci sequence with the spherical coordinate system, we established a formula to calculate the latitude and longitude of each particle.

$$\theta_n = \arccos\left(1 - \frac{2n}{N}\right) \tag{11a}$$

$$\phi_n = \pi(1+\sqrt{5})n \tag{11b}$$

where θ_n and ϕ_n are the latitude and longitude of the n-th particle, N is the total number of particles. This method allows for a more accurate representation of the spherical boundary, eliminating the roughness and irregularities inherent in the grid-based approach. As a result, this method provides a visually smoother and structurally coherent boundary for the spherical liquid tank, as illustrated in Fig. 1(b).

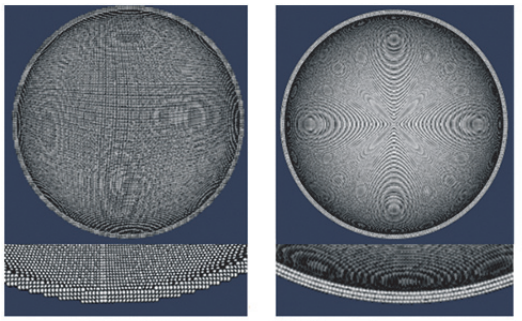

Fig. 1 Schematic diagram of the pre-processed model

2. Numerical simulation

In this paper, we investigate the sloshing phenomena in a spherical liquid tank when the fill ratio is $h/R=0.8$, specifically under conditions where the excitation frequency equals the natural frequency of the liquid. The natural frequency of the liquid is determined through the observation of its free decay sloshing behavior. Initially, the liquid surface inside the spherical tank is set at a 5° inclination, and then it undergoes a free decay motion in the absence of any external force excitation. The time history of the centroid coordinates of the liquid undergoing free decay motion is recorded, as shown in Fig. 2.

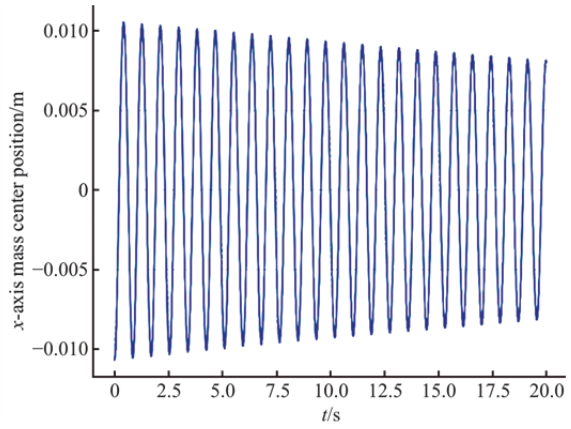

Fig. 2 (Color online) Centroid curve of free decay sloshing in a spherical liquid tank

The calculation for the damping based on the logarithmic decay rate of free decay is given by the following formula

$$\gamma=\frac{1}{2\pi n}\ln\left(\frac{A_i}{A_{i+n}}\right) \tag{12}$$

where A_i is the amplitude corresponding to the i-th wave peak, A_{i+n} is the amplitude corresponding to the $i+n$-th wave peak, n is the number of intervals between two peaks. The natural frequency of the free decay can be obtained through a weighted average of the time intervals between different peaks or troughs. Using the time history curve of the free decay centroid motion, the natural frequency of the liquid at a water depth of $h/R=0.8$ is calculated to be 1.18 Hz. Following this, we simulate the sloshing phenomena of the liquid inside the spherical tank at this excitation frequency.

To validate the accuracy of the MPS numerical method in simulating the sloshing phenomena of liquid tanks, we conduct model experiments under the same conditions and recorded the forces exerted on the tank. The experimental setup is illustrated in Fig. 3. 3-D force sensors are employed to measure the overall load, with the sensor placement shown in Fig. 4. The sensors operated at a sampling frequency of 400 Hz with a resolution of 0.01 N. Prior to the experiments, a no-load sloshing test of the spherical tank is conducted to determine the inertial forces of the tank and its external supports. Subsequently, the same excitation test was conducted with the tank filled, and the measured forces minus the inertial forces were considered as the actual sloshing forces exerted on the tank.

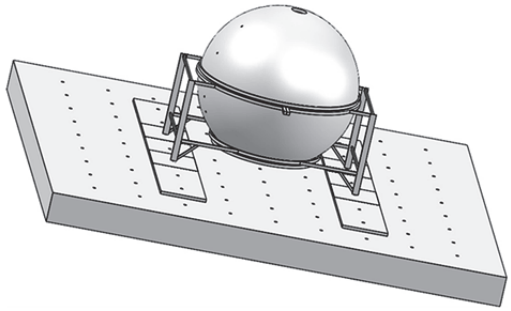

Fig. 3 Schematic of the experimental setup

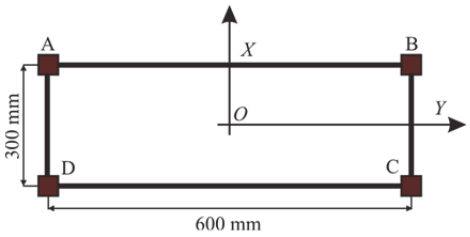

Fig. 4 (Color online) Layout of force sensors on the experimental setup

Despite calibration of the force measurement points, the results obtained from experimental methods are inevitably subject to errors. Therefore, for

further validation, a mesh-based numerical method is employed as a comparison. The OpenFOAM open-source program is used, implementing the FVM method to simulate sloshing in the spherical tank under the same conditions. The results obtained by the three methods are compared as follows.

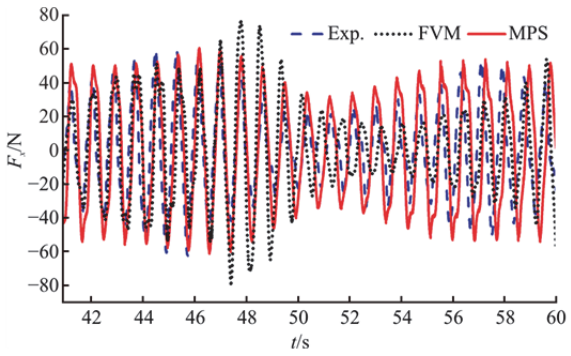

Fig. 5 (Color online) Comparison of force-time history curves of the tank

The time history curves of the sloshing forces obtained by the three methods are shown in Fig. 5. These curves demonstrate good temporal consistency across the methods, validating the accuracy of the MPS approach. Notably, the MPS method results align more closely with experimental data and exhibit smaller errors compared with the FVM method. The frequency domain curves are obtained by FFT transformation, as shown in Fig. 6. In the frequency domain, the MPS method also shows superior consistency with the experimental results, particularly in terms of spectral peak frequency and peak values. Conversely, the results derived from the FVM method display some discrepancies. This indicates that the MPS method has distinct advantages in simulating free-surface large deformation problems, capturing the free liquid surface more accurately and yielding results that are more congruent with experimental results.

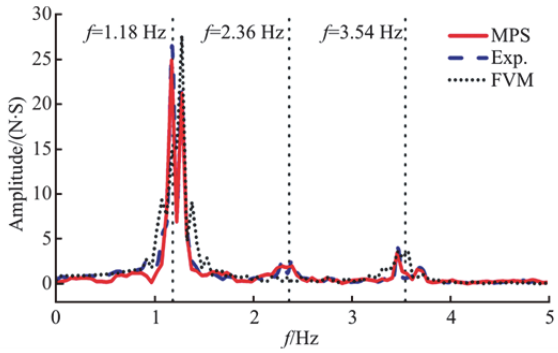

Fig. 6 (Color online) Comparison of frequency domain curves of the forces on the tank

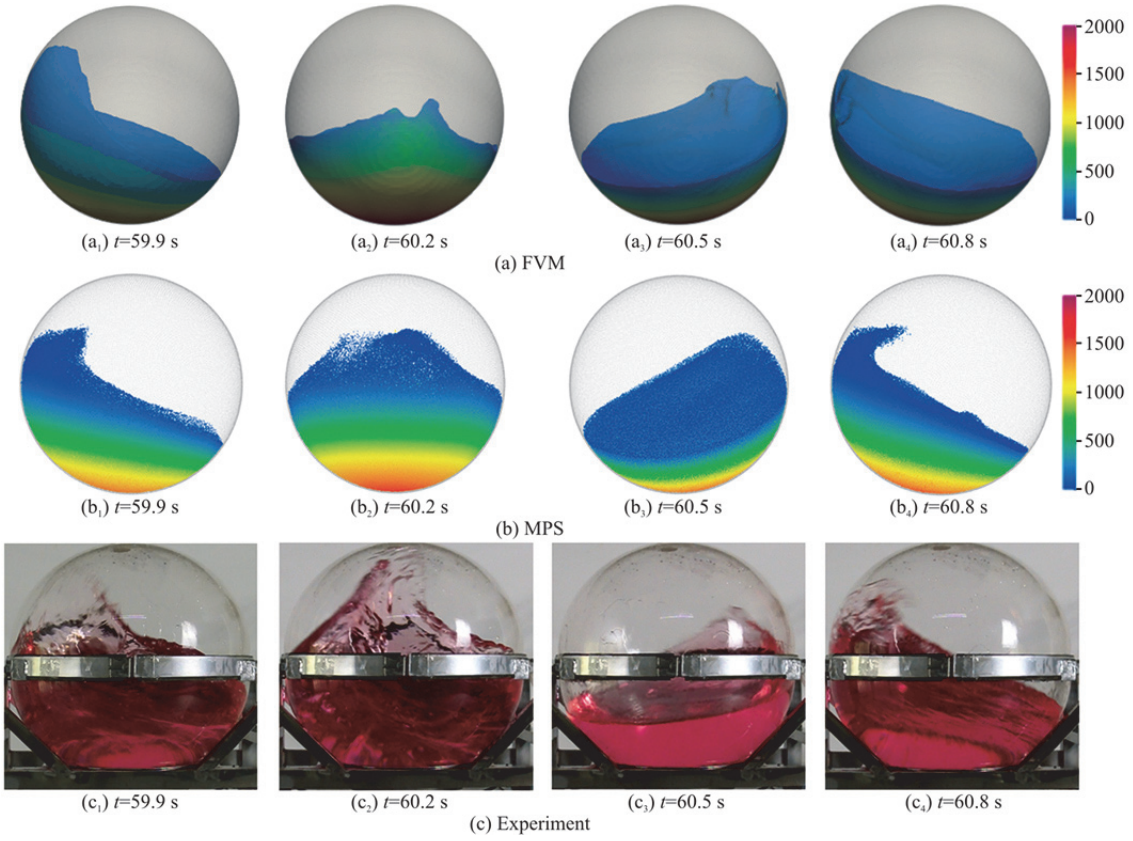

Fig. 7 (Color online) Comparison of free surface shape of spherical tank

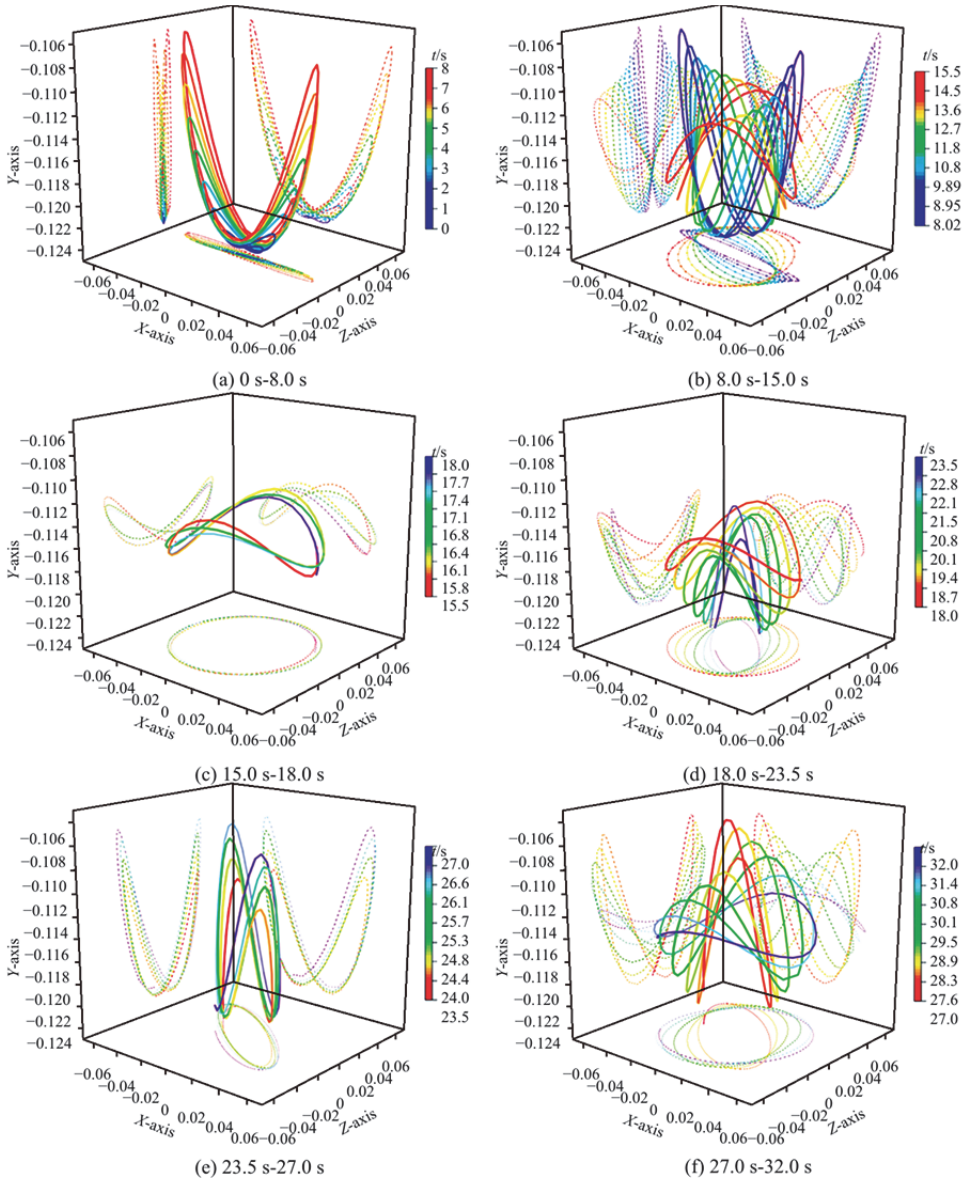

Fig. 8 (Color online) Trajectory lines of the liquid centroid

It can be seen from frequency domain curves in Fig. 6 that the primary response of the sloshing forces in the liquid tank is concentrated around the first-order natural frequency, with spectral peaks also occurring near this frequency. However, as shown in Fig. 6, smaller peaks are observed near the second and third multiples of the natural frequency in the frequency domain curves, which warrants further discussion. These peaks can be attributed to several phenomena. (1) harmonic responses, which are integer multiples of the fundamental frequency, may arise due to the system being excited at its first-order natural frequency. Such harmonics are a common occurrence in dynamic systems subjected to periodic forces. (2) nonlinear effects within the system can generate additional frequency components, manifesting as these lesser peaks in the frequency spectrum. These nonlinearities, especially prevalent in systems with large free surface deformations, can significantly alter the response behavior. It is plausible that these observed peaks represent harmonics or nonlinear responses rather than higher-order natural frequencies.

Figure 7 presents a comparative analysis of the liquid's free surface shapes as derived from three different methods. The experimental results indicate that under resonant frequency excitation, the liquid exhibits pronounced non-linear behaviours. A particularly noteworthy observation is the rotational motion of the liquid within the spherical tank when subjected to horizontal excitation. Both mesh-based and mesh-free methods effectively captured the liquid's rotational dynamics. However, in replicating the more

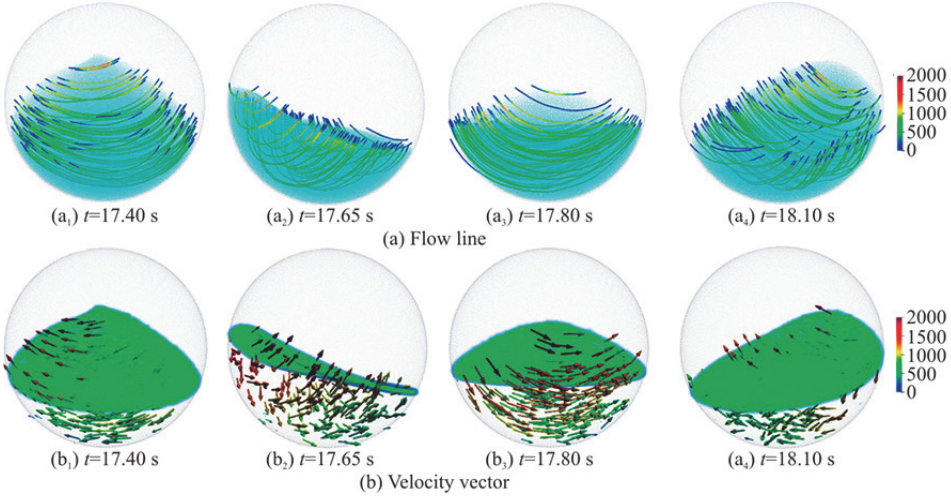

Fig. 9 (Color online) Velocity distribution of flow field

complex aspects, such as intense rolling and surface breaking, the mesh-based FVM fell short in accuracy, whereas the MPS method adeptly simulated the splashing and droplet formation. This comparative study underscores the superior capability of the mesh-free particle method in handling intricate fluid dynamics scenarios.

Next, we analyze the rotational motion, focusing on the trajectory of the liquid's centroid. The trajectory lines reveal six distinct motion patterns under horizontal excitation at the resonance frequency.

Initial oscillation (Fig. 8(a)): The liquid oscillates along the excitation direction, with increasing amplitude over time. The trajectory is nearly linear in the X-Z and Y-Z planes but forms a U-shape in the X-Y plane.

Transition to pendulum motion (Fig. 8(b)): The amplitude decreases and shifts clockwise. The X-Z plane trajectory evolves from linear to elliptical, eventually forming a circular base, while the X-Y and Y-Z planes show diminishing trajectories, ultimately creating a "8" pattern.

Stabilized sloshing (Fig. 8(c)): This phase is marked by stability, with overlapping trajectory lines over three periods. In the X-Z plane, the trajectory is circular, while in the X-Y and Y-Z planes, it forms a "8", resembling a three-dimensional saddle shape.

Saddle shape modification (Fig. 8(d)): The saddle-shaped trajectory starts folding downwards, and the circular X-Z plane trajectory reverts to an elliptical shape. The ellipse's major axis rotates counterclockwise, aligning at a 45° angle to the x-axis.

pendulum motion at an angle (Fig. 8(e)): The trajectory stabilizes in a pendulum motion at a 45° angle to the X-axis, with increasing amplitude. The projections in the X-Z plane nearly coincide, while amplitude in the X-Y and Y-Z planes progressively increases.

Amplitude Reduction (Fig. 8(f)): As the amplitude reaches its peak along the ellipse's major axis, the amplitude in the gravity direction begins to decrease. The X-Z plane trajectory shifts clockwise, with the minor axis elongating to form a circle, while the horizontal amplitude remains nearly constant.

To delve deeper into the flow field during tank sloshing, streamline distribution diagrams and the velocity vector of the flow field are plotted as shown in Fig. 9. These diagrams reveal that even at moments when the entire flow field exhibits rotational motion, the streamlines are distributed following the trajectory of a simple pendulum motion, rather than all particles in the field executing circular motions around a vertical axis.

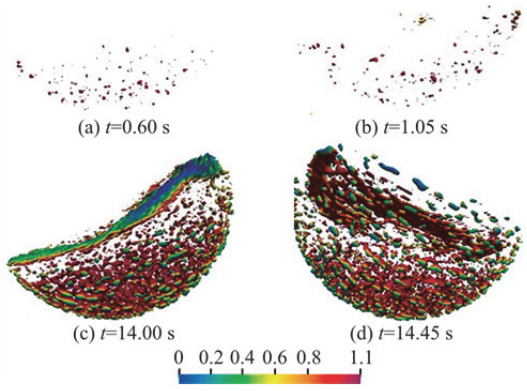

Fig.10 (Color online) Schematic of the vortex of the flow field

The flow field of such intense, vortex-like motions suggests the formation of distinct vortex structures. By employing the Q-criterion in Paraview, we

generated vortex structure distribution diagrams for the flow field, as illustrated in Fig.10. These diagrams reveal that during the initial phase of relatively gentle flow motion, only a few small vortex structures are present. However, with the escalation of sloshing intensity, vortex structures proliferate throughout the flow field. Remarkably, these structures are not limited to the vicinity of the free surface but are evenly distributed across the entire field. This uniform distribution highlights that during intense sloshing and strong non-linear movements, fluid overturning occurs not just near the surface but throughout the flow field.

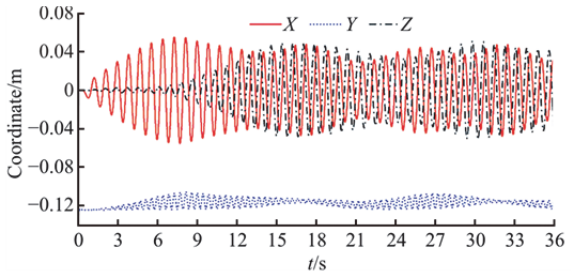

Fig. 11 (Color online) Time history curve of fluid centroid position

Figure 11 shows the time history curves of the centroid's coordinates in the X-, Y-, Z-directions. Initially, the fluid sloshes predominantly along the X-axis, exhibiting minimal amplitudes in the Y and Z axes. Around the 8-second mark, notable sloshing along the Z-axis begins to develop. Between 15.0 s-18.0 s, the reciprocal amplitudes in the X- and Z-directions reach their zenith, agreeing with the circular projection of the liquid's trajectory in the X-Z plane, as shown in Fig. 8(c). Notably, when the X-Z direction amplitudes simultaneously peak, the amplitude in the Y-axis is minimized, which can be interpreted through the lens of energy conservation.

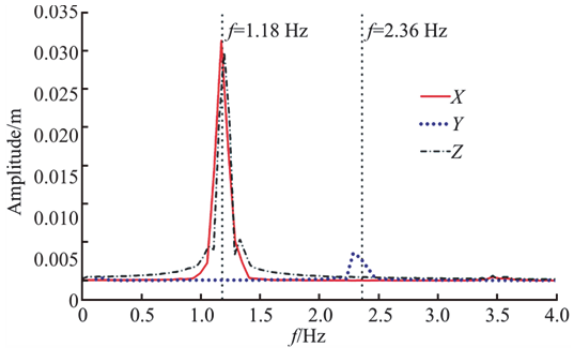

Fig. 12 (Color online) Frequency domain curve of fluid centroid position

The fluid centroid's frequency domain curves are shown as Fig. 12. It can be seen that the spectral peak values in the X- and Z-directions are significantly higher than those in the Y-direction, indicating that the primary sloshing motion of the liquid predominantly occurs in the X- and Z-directions. Besides, the frequency peaks of the centroid's motion in the X- and Z-directions align with the fluid's natural frequency. Conversely, in the Y-direction, the sloshing frequency's spectral peak is observed near the double of the natural frequency. This behaviour is similar to Faraday waves in vertical sloshing scenarios, as previously documented in literature[27-28], where the intrinsic sloshing frequency is twice the natural frequency. Our simulations, under horizontal excitation at the natural frequency, show a similar pattern with the liquid's response frequency along the gravity direction occurring at double the natural frequency.

3. Conclusion

In this paper, the sloshing phenomena within a spherical liquid tank were simulated using the mesh-free particle method (MPS), and its accuracy was validated against experimental data and the FVM. The comparisons indicate that the MPS method aligns more closely with experimental outcomes, suggesting that mesh-free particle-based approaches have a distinct advantage in modelling such strongly non-linear problems. When subjected to excitation at its natural frequency, the liquid demonstrated vigorous sloshing motion and entered a rotational state. The trajectory of the fluid centroid revealed six distinct characteristic motion modes. Streamline drawings indicated that the movement of the fluid in the flow field primarily resembled a simple pendulum, as opposed to rotational motion around a longitudinal axis. Vortex structure distribution maps showed that vortices were uniformly distributed throughout the flow field, not just near the free surface. Time history curves of the fluid centroid's position, coupled with frequency domain analysis, revealed that the response frequency of the centroid in the X- and Z-directions equals to the natural frequency, while the response in the Y-direction was twice the natural frequency.

Acknowledgement

(This research received other funding agency in the public, commercial, or not-for-profit sectors.)

Compliance with ethical standards

Conflict of interest: The authors declare that they have no conflict of interest. De-cheng Wan is editorial board member for the Journal of Hydrodynamics and was not involved in the editorial review, or the

decision to publish this article. All authors declare that there are no other competing interests.

Ethical approval: This article does not contain any studies with human participants or animals performed by any of the authors.

Informed consent: Not application.

References

[1] Lu Y., Yue B. Z., Ma B. L. et al. Moving pulsating ball equivalent model and its validation experiment for large amplitude liquid slosh in gravity environment [J]. *Chinese Journal of Theoretical and Applied Mechanics*, 2022, 54(9): 2543-2551.

[2] Ding S. L., Bao G. W. Modal analysis and equivalent mechanical model of liquid sloshing in arbitrary 3D container [J]. *Chinese Quarterly of Mechanics*, 2004, 25(1): 62-68.

[3] Liu Z., Yuan K., Liu Y. et al. Fluid sloshing hydrodynamics in a cryogenic fuel storage tank under different order natural frequencies [J]. *Journal of Energy Storage*, 2022, 52: 104830.

[4] Furuichi Y., Himeno T., Watanabe T. et al. Evaluation of sloshing effect on a tank during landing phases of spacecrafts in a micro-gravity environment [C]. *ASCEND 2022*, Las Vegas, Nevada, USA, 2022.

[5] Hari M. D., Sarigul-Klijn N. Sloshing behavior in rigid and flexible propellant tanks: computations and experimental validation [J]. *Journal of Spacecraft and Rockets*, 2021, 58(1): 100-109.

[6] Yang H. Q., Peugeot J. Propellant sloshing parameter extraction from computational-fluid-dynamics analysis [J]. *Journal of Spacecraft and Rockets*, 2014, 51(3): 908-916.

[7] Chiba M., Motoyama N., Shigematsu S. Theoretical and experimental study on the effect of plane diaphragm tension on dynamic stability of liquid in a hemispherical tank under vertical excitation [J]. *Journal of Fluids and Structures*, 2023, 120: 103905.

[8] Li D., Xiao H., Jin Y. Design optimization of sloshing tank using weakly compressible mesh free model [J]. *Ocean Engineering*, 2023, 284: 115218.

[9] Martinez-Carrascal J., Pizzoli M., Saltari F. et al. Sloshing reduced-order model trained with Smoothed Particle Hydrodynamics simulations [J]. *Nonlinear Dynamics*, 2023, 111: 21099-21115.

[10] Green M. D., Zhou Y., Dominguez J. M. et al. Smooth particle hydrodynamics simulations of long-duration violent three-dimensional sloshing in tanks [J]. *Ocean Engineering*, 2021, 229: 108925.

[11] Kotsarinis K., Green M. D., Simonini A. et al. Modeling sloshing damping for spacecraft: A smoothed particle hydrodynamics application [J]. *Aerospace Science and Technology*, 2023, 133: 108090.

[12] Koshizuka S., Oka Y., Tamako H. A particle method for calculating splashing of incompressible viscous fluid [C]. *International Conference, Mathematics and Computations, Reactor Physics, and Environmental Analyses*, Portland, 1995, 1514-1521.

[13] Zhang G., Zha R., Wan D. MPS–FEM coupled method for 3D dam-break flows with elastic gate structures [J]. *European Journal of Mechanics/B Fluids*, 2022, 94: 171-189.

[14] Chen X., Wan D. Numerical simulation of three-dimensional violent free surface flows by GPU-Based MPS method [J]. *International Journal of Computational Methods*, 2019, 16(4), 1843012.

[15] Zhang Y., Wan D. MPS-FEM coupled method for fluid–structure interaction in 3D dam-break flows [J]. *International Journal of Computational Methods*, 2019, 16(2): 1846009.

[16] Zha R., Zhao W., Wan D. Numerical study on water entry of projectiles with various head shapes by a multiphase moving particle semi-implicit method [J]. *International Journal of Offshore and Polar Engineering*, 2022, 32(4): 402-410.

[17] Huang C. Y., Zhang G. Y., Wan D. C. Hydroelastic responses of an elastic cylinder impacting on the free surface by MPS-FEM coupled method [J]. *Acta Mechanica Sinica*, 2022, 38(11): 322057.

[18] Zhang Y., Wan D. MPS-FEM coupled method for sloshing flows in an elastic tank [J]. *Ocean Engineering*, 2018, 152: 416-427.

[19] Xie F. Z., Meng Q. J., Wan D. C. Numerical simulations of liquid-solid flows in a vertical pipe by MPS-DEM coupling method [J]. *China Ocean Engineering*, 2022, 36: 542-552.

[20] Zhang G., Zhao W., Wan D. moving particle semi-implicit method coupled with Finite Element Method for hydroelastic responses of floating structures in waves [J]. *European Journal of Mechanics /B Fluids*, 2022, 95: 63-82.

[21] Pan X. J., Xie F. Z., Wan D. C. Numerical analysis of influence of liquid velocity on characteristics of vertical pipe transportation by MPS-DEM method [J]. *Chinese Journal of Hydrodynamics*, 2021, 36(6): 835-842(in Chinese).

[22] Zha R., Zhao W., Wan D. Numerical study of wave-ice floe interactions and overwash by a meshfree particle method [J]. *Ocean Engineering*, 2023, 286: 115681.

[23] Huang C. Y., Zhao W. W., Wan D. C. Simulation of the motion of an elastic hull in regular waves based on MPS-FEM method [J]. *Chinese Journal of Theoretical and Applied Mechanics*, 2022, 54(12): 3319-3332.

[24] Wen X., Zhao W., Wan D. Multi-phase moving particle semi-implicit method for violent sloshing flows [J] *European Journal of Mechanics /B Fluids*, 2022, 95: 1-22.

[25] Wen X., Zhao W. W., Wan D. C. Numerical simulations of multi-layer-liquid sloshing by multiphase MPS method [J]. *Journal of Hydrodynamics*, 2021, 33(5): 938-949.

[26] Xie F., Zhao W., Wan D. MPS-DEM coupling method for interaction between fluid and thin elastic structures [J]. *Ocean Engineering*, 2021, 236: 109449.

[27] Zhang G. Y., Zhao W. W., Wan D. C. Numerical simulations of sloshing waves in vertically excited square tank by improved MPS method [J]. *Journal of Hydrodynamics*, 2022, 34(1): 76-84.

[28] Huang C. Y., Zhao W. W., Wan D. C. Numerical simulations of faraday waves in cylindrical and hexagonal tanks based on MPS method [J]. *Journal of Hydrodynamics*, 2023, 35(2): 278-286.

[29] Tanaka M., Masunaga T. Stabilization and smoothing of pressure in MPS method by quasi-compressibility [J]. *Journal of Computational Physics*, 2010, 229(11): 4279-4290.

[30] Lee B., Park J., Kim M. et al. Step-by-step improvement of MPS method in simulating violent free-surface motions and impact-loads [J]. *Computer Methods in Applied Mechanics and Engineering*, 2011, 200(9-12): 1113-1125.